JACS Au
AN OPEN ACCESS JOURNAL OF THE AMERICAN CHEMICAL SOCIETY

pubs.acs.org/jacsau
Article

L-2,3-Diaminopropionate Binding Mode of the SulM Adenylation Domain Limits Engineering Monobactam Analogue Biosynthesis with Larger Substrates

Lukas Kahlert,[§] Ketan D. Patel,[§] Michael S. Lichstrahl, Rongfeng Li, Chengkun He, Andrew M. Gulick,* and Craig A. Townsend*

Cite This: JACS Au 2025, 5, 1992−2003
Read Online

ACCESS | Metrics & More | Article Recommendations | Supporting Information

ABSTRACT: The simple but essential azetidinone core of the β-lactam antibiotics is uniquely N-sulfonated in the monobactam subfamily. This feature confers both target binding specificity to inactivate bacterial cell wall biosynthesis (antibiosis) and structural differentiation to elude destruction by metallo-β-lactamases (MBLs). The recent FDA approval of Emblaveo to treat serious bacterial infections combines an established synthetic monobactam aztreonam and avibactam, which additionally blocks serine β-lactamases, to create a broadly effective antibacterial therapeutic. Here we report experiments to capture the native monobactam biosynthetic steps to the natural product sulfazecin with the aim of accessing new monobactams by reprogramming its biosynthetic machinery. In sulfazecin biosynthesis, the β-lactam ring is formed by a nonribosomal peptide synthetase SulM that incorporates L-2,3-diaminopropionate (Dap), which is then N-sulfonated in trans and efficiently cyclized to the fully elaborated monobactam by an unusual thioesterase (TE) domain. We describe an improved synthesis of (2*S*,3*R*)-vinylDap to support rational structure-based engineering experiments to obtain the corresponding (4*R*)-vinyl sulfazecin. While these experiments were initially based on an AlphaFold model of the adenylation domain that incorporates Dap (SulM A3), we further report high-resolution X-ray crystal structures with both the L-Dap substrate and an accurate analogue of the activated (3*R*)-methyl-Dap adenylate bound. The ligand-bound structures rationalize the inability of SulA3 to incorporate larger substrates. Comparisons with the structures of other diamino acid-activating adenylation domains identify alternate binding modes that may be more suitable for the production of sulfazecin analogues. The impact of these structures on the further engineering of the SulA3 domain and its relation to monobactam synthesis in the recently structurally characterized SulTE are discussed.

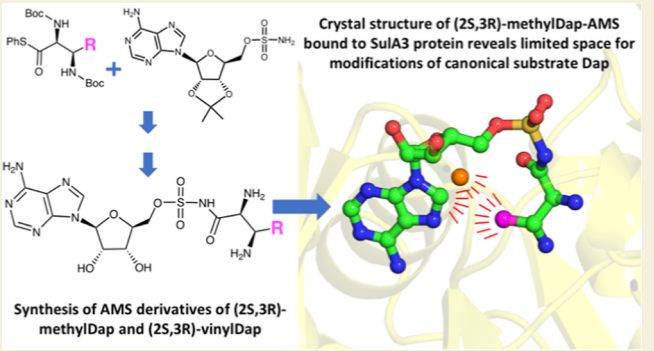

KEYWORDS: *β-lactam, nonribosomal peptide synthetase, monobactam, NRPS, bacterial, biosynthesis, sulfazecin, SulM, adenylation, SulA3*

The often lax substrate selectivity of native natural product biosynthetic enzymes opens the door to application of mutasynthesis methods[1−5] to capture the scale and efficiency of modern fermentation technology for the production of rationally modified natural products.[6,7] In its most effective incarnation, if the formation of a key biosynthetic intermediate can be blocked by gene deletion or inactivation, then simple supplementation of the growth medium with a structural analogue of this essential intermediate can often be taken up by the biosynthetic machinery to produce *only* the variant of the natural product. A recent proof-of-concept experiment demonstrated how this approach can be applied to prepare derivatives of the β-lactam antibiotic sulfazecin (**3**).[8] Here one of the two enzymes (SulG) required to synthesize L-2,3-diaminopropionate (**2**, Dap) from the primary metabolite L-3-phosphoserine[9−11] was inactivated, and Dap synthetic derivatives (2*S*,3*R*)-methyl-Dap (**4**) and -fluoromethyl-Dap (**5**) were successfully incorporated in vivo into sulfazecin analogues **6** (R = CH_3) and **7** (R = CH_2F); see Scheme 1A.[8]

Sulfazecin is biosynthesized through the activity of a pair of modular nonribosomal peptide synthetase (NRPS) enzymes (SulI and SulM, Scheme 1B) that incorporate peptidyl carrier proteins (PCPs) and catalytic domains in large multidomain enzymes.[12−14] The fact that sulfazecin analogues can be constructed through precursor-directed biosynthesis means that the adenylation domain of the third module (designated,

Received: March 4, 2025
Revised: April 9, 2025
Accepted: April 10, 2025
Published: April 16, 2025

Scheme 1. (A) Preparation of Structural Analogues of the β-Lactam Antibiotic Sulfazecin by Application of Mutasynthetic Methods to (B) the Native Sulfazecin Biosynthetic Pathway[a]

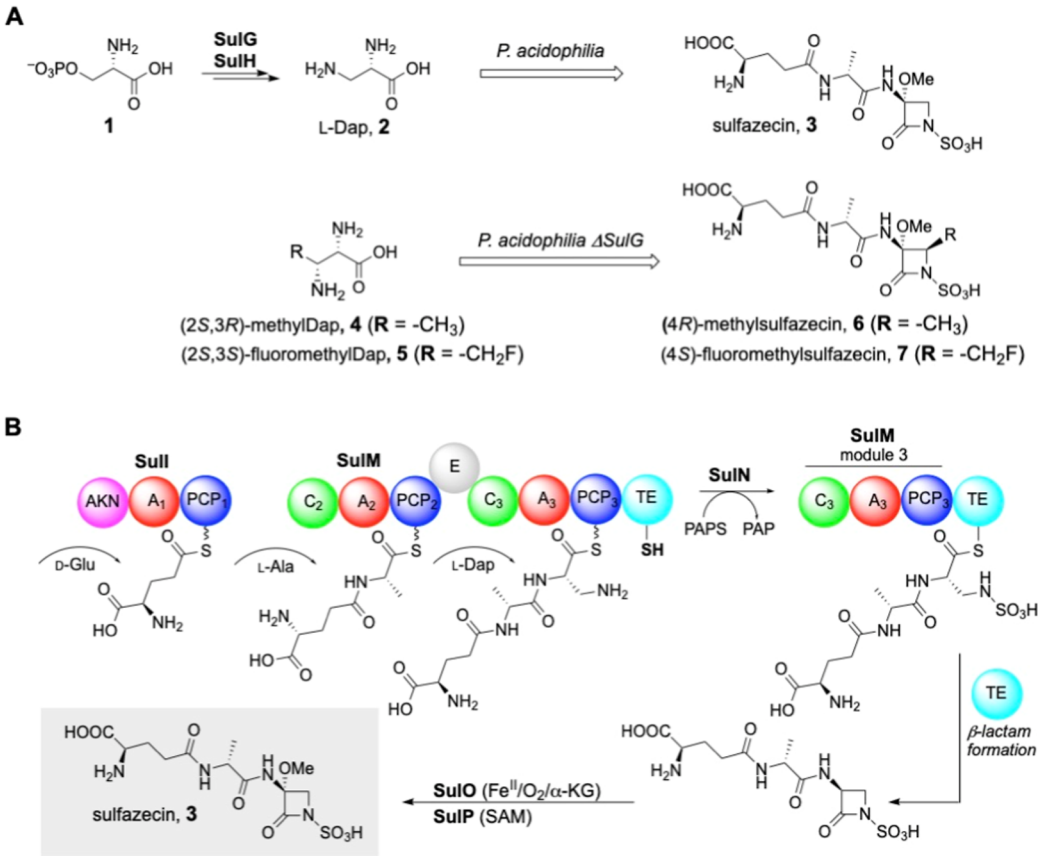

[a]Biosynthetic domains are represented as A, adenylation; PCP, peptidyl carrier protein; C, condensation; E, epimerization; TE, thioesterase; and AKN, adenylyl sulfate kinase.

Scheme 2. (A) Potential Isostere of the C-Terminal N-Sulfonated Tripeptide Intermediate in Sulfazecin Biosynthesis Depicted in Scheme 1B; (B) Overview of the Synthesis of (2S,3R)-VinylDap and (2S,3R)-AlkynylDap

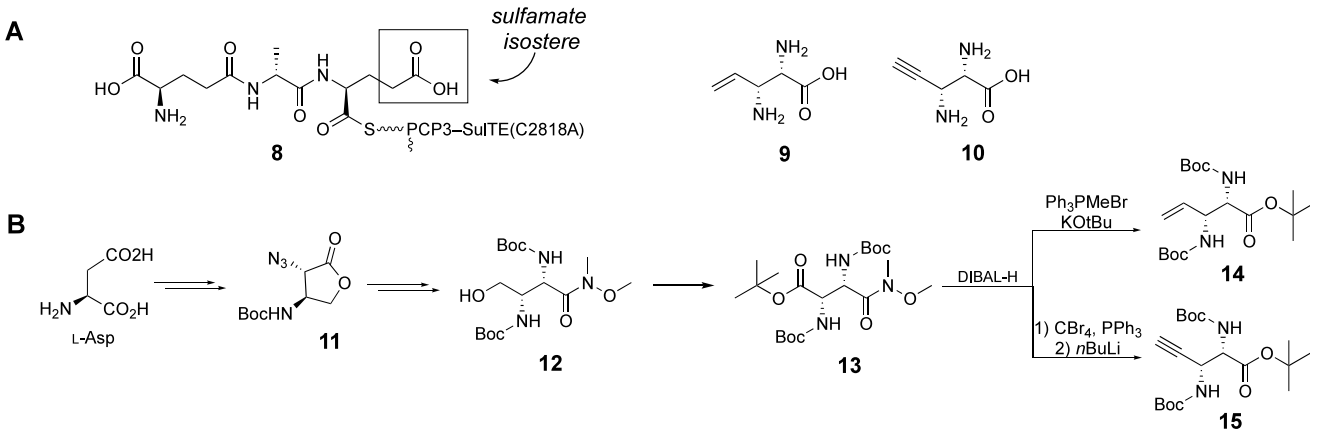

SulA3) of SulM recognized and activated the Dap analogues with ATP for transport by the peptidyl carrier protein of module 3 (PCP3) and amide bond formation. Presentation of the PCP3-Dap analogue in the intervening condensation domain (SulC3) enables the upstream D-γ-Glu—D-Ala—PCP2 dipeptide to condense in a defined manner to afford the D,D,L-tripeptide linked to PCP3, as shown schematically in Scheme 1B. SulN catalyzes in trans N-sulfonation with PAPS[9,10] to produce the sulfamate for delivery into the C-terminal thioesterase (SulTE) domain. SulTE, bearing an active site Cys rather than a conventional catalytic Ser residue, catalyzes N-sulfonated monocyclic β-lactam (monobactam) ring formation with deft overall synthetic efficiency. Crystal structures have been published recently[15] of both the TE alone and the didomain complex of PCP3−SulTE bearing the phosphopantetheine cofactor loaded with a tripeptide mimic bearing a terminal carboxylate of L-Glu in **8** (see Scheme 2A). This ligand was chosen as an approximate isostere of the negatively

https://doi.org/10.1021/jacsau.5c00231
JACS Au 2025, 5, 1992−2003

charged N-sulfonated L-Dap in the native substrate, although the peptide was not resolved in the final structure. Molecular modeling and comparisons to the structure of the mechanistically closely related β-lactone forming TE in obafluorin biosynthesis[16,17] identified corresponding oxyanion holes that help mediate strained β-lactam/β-lactone formation and give detailed pictures of how monobactam synthesis and concomitant release occur.[15]

Advances in medicinal chemistry have independently established that simple substitutions at the monobactam (4*R*)-position confer an improved spectrum of antibiotic activity.[18,19] As a first step along the path to building out functionality at this key locus, we developed a versatile synthesis of L-Dap analogues for testing as potential substrates.[8] Mutasynthesis experiments in a Δ*sulG* knockout, which is incapable of L-Dap synthesis, demonstrated that (2*S*,3*R*)-methylDap (**4**) and (2*S*,3*S*)-fluoromethylDap (**5**) were bound and activated in vivo by SulA3 and proceeded through all subsequent synthetic steps to give **6** and **7**, respectively. Additionally, (3*R*)-vinylDap (**9**) was of particular interest to enable myriad synthetic options available to diversify the double bond to produce more variants of sulfazecin. In the course of assembling a small library of (3*R*)-substituted L-Dap derivatives for these mutasynthesis studies, vinylDap (**9**) and alkynylDap (**10**, Scheme 2A) were prepared from a common intermediate **13** (see Scheme 2B).[8] In contrast to our successes above, the increased bulk of a vinyl substituent gave only trace levels of ATP activation in SulA3.[8] We reasoned that limited activity with SulA3 and (3*R*)-vinylDap (**9**) could potentially be overcome through a structure-guided effort to expand the active-site pocket of the SulA3 adenylation domain. We report here the synthesis of Dap analogues, our initial efforts to produce mutations in SulA3 to accommodate the larger substrates, and structures of the SulA3 core domain in the presence of modified ligands that highlight the challenges with adenylation domain engineering.

METHODS

Protein Production and Purification

Native and mutant A_3-PCP_3 didomain was expressed in *Escherichia coli* Rosetta 2 (DE3) and purified by Ni^{2+}-affinity chromatography as described earlier.[20] Selected mutants of the A_3-PCP_3 didomain[9,20] were generated using the Q5 site-directed mutagenesis kit (New England Biolabs) according to the manufacturer's protocol. Primers are listed in Table S1.

Cloning and Expression of the SulA3 N-Terminal Subdomain

The N-terminal subdomain of SulA3 (NCBI Accession: WP_096724622, Pro2124−Lys2545) was cloned using TEV-sulA3N-F and -R primers (Table S1). The *sulA3N* fragment was amplified, and the PCR product was assembled into *Nde*I−*Hind*III digested pET28bTEV (Novagen, Madison, WI) using New England Biolabs (Cambridge, MA) 2× Hi-Fi DNA Assembling Mix to generate expression construct pET28bTEV/sulA3N.

To express TEV-SulA3N, pET28bTEV/sulA3N was transformed into *E. coli* Rosetta 2 (DE3) cells by electroporation. To express TEV-SulA3N, 5 L of LB + 1% glycerol medium containing 50 mg/mL kanamycin and 50 mg/mL chloramphenicol in a bioreactor was inoculated with 50 mL of overnight seed culture. The culture was grown at 37 °C to OD_{600} = 0.65 and cold-shocked with ice water for 40 min. The expression was induced with 0.5 mM isopropyl β-D-thiogalacto-pyranoside (IPTG), and growth continued at 18 °C for 24 h.

TEV-SulA3N was first purified by Ni-NTA chromatography, and the purified protein was exchanged into 50 mM Tris−HCl (pH 8.0) and 5% glycerol buffer. The TEV tag was cleaved by incubating 270 mg of TEV-SulA3N with 8 mg of purified SuperTEV protease expressed from pET28b/TEV. The cleavage reaction was carried out overnight at 4 °C with slow rotation. The protein mixture was subjected to another Ni-NTA chromatography, and the tagless SulA3N protein was collected in the flowthrough.

Adenylation Domain In Vitro Assays

The relative activity of the native and mutant A_3-PCP_3 didomain was determined spectrophotometrically by the ferric iron/hydroxylamine-based in vitro assay as described earlier with minor modifications.[20] Each sample contained 50 mM Tris−HCl pH 8.5, 10 mM magnesium chloride, 10 mM ATP, 150 mM hydroxylamine (prepare a 2 M stock solution by dissolving hydroxylamine hydrochloride in 2 M sodium hydroxide, adjust the pH to approximately 7.5), and a 5 μM adenylation domain in a total volume of 100 μL. The reaction was started by addition of 6 mM amino acid substrate; no amino acid was added to the reference samples. After incubation for 18 h at 30 °C, samples were quenched with 100 μL of 0.7 M hydrochloric acid containing 10% (w/v) iron(III) chloride (Sigma-Aldrich) and 3.3% (w/v) trichloroacetic acid (J. T. Baker). Samples were centrifuged (14,500*g*, 4 min), and the absorbance of the clear supernatant was measured at 490 nm on a Cary 50 UV−vis spectrophotometer (Varian).

Crystallization of Proteins

IMAC-purified and TEV-digested protein was further subjected to gel filtration using a Sephadex S200 16 mm × 300 mm column in a buffer containing 25 mM HEPES, 150 mM NaCl, and 0.5 mM TCEP, pH 7.5. Protein was concentrated to 15 mg/mL for storage at −80 °C. Crystallization screening was performed at 10 mg/mL. Sparse matrix screens MCSG-1 and Index (Hampton Research) yielded crystals under several conditions. Crystallization was further optimized in a 24-well hanging drop plate at 10 mg/mL in the Index condition comprising 0.1 M HEPES, 0.2 M $MgCl_2$, and 25% PEG3350. Co-crystallization with ligands L-Dap and methyl-Dap-AMS was performed under similar conditions with 2.5 mM ligand concentration and protein at 10 mg/mL. SulA3_N and L-Dap cocrystals were cryo-protected through serial transfers in crystallization cocktail supplemented with 8%, 16%, and 24% glycerol. Similarly, SulA3-methyl-Dap-AMS cocrystals were cryo-protected with crystallization cocktail supplemented with 8%, 16%, and 24% of a solution containing 200 mg/mL NDSB-201 [3-(1-pyridinio)-1-propanesulfonate] and 60% ethylene glycol. Cryo-protected crystals were flash-frozen in liquid nitrogen.

Structure Solution of the L-Dap-Bound and Methyl-Dap-AMS-Bound SulA3 Core Domain

Remote data collection from single crystals was conducted at the SSRL and APS beamlines. Data processing was performed with iMosflm. The SulA3-L-Dap cocrystal data set was processed to a resolution of 1.55 Å in space group $P2_12_12$, while the SulA3-methyl-Dap-AMS cocrystal data set was processed to 1.30 Å. The SulA3-L-Dap cocrystal structure solution was performed by molecular replacement using the AlphaFold2 model as a search model in the Phaser module of Phenix.[21,22] Model building and iterative refinements were carried out with Coot[23] and Phenix.refine. The SulA3-L-Dap cocrystal structure was used as a search model in molecular replacement for the SulA3-methyl-Dap-AMS cocrystal structure solution, which was similarly refined. Omit map electron densities for the ligands in both structures are presented in Figure S1. Final statistics for data collection and refinement are presented in Table S2.

RESULTS

Structure-Based Engineering of SulA3 to Accommodate (3*R*)-Methyl-Dap (4) and (3*R*)-Vinyl-Dap (9)

With synthetic access to vinylDap (**9**), we generated an AlphaFold2[24] model of SulA3 and modeled its native substrate

https://doi.org/10.1021/jacsau.5c00231
JACS Au 2025, 5, 1992−2003

L-Dap, the simplest diamino acid, into the active site. The model provided a preliminary assessment of the structure and relatively high confidence in the proximity of residues to the binding pocket. With the goal in mind to remodel SulA3 to accommodate Dap analogues having small hydrophobic substituents at its 3*R* position (e.g., methyl, vinyl), first- and second-sphere residues were identified for the preparation of variants to potentially accomplish this aim. The broader screening of active-site residues was initiated with the hope that ligand-bound experimental structures could inform and guide a second set of mutants.

To narrow down the number of targeted positions for "rational" mutagenesis experiments, we decided to focus on the specificity-conferring adenylation domain residues[25,26] as these positions have been reported to be the most promising sites for engineering efforts.[27,28] We hypothesized that accommodation of additional hydrophobic bulk at the (3*R*)-position might benefit from an enlarged active site cavity. Based on the structural model, Val2238, which appears to be opposed to the Dap (3*R*)-substituent, and Trp2341, positioned behind Val2238, were exchanged for smaller amino acids to construct V2238G, W2341F, and the double mutants V2238G/W2341F and V2238A/W2341F. None of these A3 variants showed a notable increase in adenylating activity with the non-native substrate (3*R*)-vinylDap, and all were also less active on the native substrate L-Dap (data not shown). Asn2411 was identified as another residue that could potentially interact with or clash with a larger (3*R*)-substituent. Among the four tested variants (N2411T/S/A/G), none exhibited elevated adenylating activity on the vinyl-Dap derivative; however, we were encouraged to see that N2411T showed both an increased relative activity on the native substrate L-Dap (ca. 18%) and a higher relative activity on the (3*R*)-methyl-analogue (ca. 64%, Figure 1). The fact that a small, rational

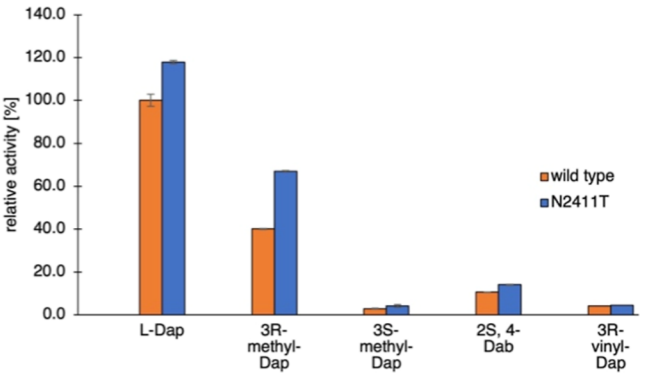

Figure 1. Analysis of SulA3 mutant adenylating activity. Relative activity of native A_3-PCP_3 and the mutant N2411T toward functionalized diaminopropionates and the nonbranched 2*S*,4-diaminobutyrate (Dab) based on the ferric iron/hydroxylamine in vitro assay.[20] All assays were performed with 5 μM enzyme and 6 mM amino substrate. Reactions were performed for 18 h at 30 °C in triplicate. Error bars indicate standard deviation.

change demonstrated improved activity suggested that additional engineering and evolution of A3 could lead to further improvement. Further, we expected that structural analysis with ligands might illustrate the precise positioning of the ligand in the active-site pocket to provide an explanation for this improvement in activity with both Dap and methyl-Dap.

To proceed further in this investigation, there were two requirements. First, a selective but more efficient synthesis of (3*R*)-vinylDap (**9**) was needed to meet the practical requirement for sufficient material to screen mutant libraries for any engineering efforts to improve substrate tolerance and flux through the biosynthetic machinery: that is, the ability of SulA3 to recognize and activate L-Dap analogues. It was understood that despite a widely sustained effort for more than two decades, reprogramming of A domains to recognize and activate non-native substrates for polypeptide elongation by NRPSs remains a formidable, largely unmet challenge.[29−33] Second, acknowledging limitations of ligand binding predictions in computational models, we pursued experimental structures bound to substrates that present the mode of binding for (2*S*,3*R*)-methylDap (**4**). These structures would reveal (see below) the extent of steric clashes in a tight binding pocket that prevents binding to larger substituted diamino acids.

Improved Synthesis of (3*R*)-VinylDap (9)

Syntheses of α,β-diamino acids such as L-Dap have been well developed and reviewed.[34] Our earlier approach summarized above in Scheme 2B relied on stereoselective C−N bond introduction to a pre-existing carbon skeleton. It was recognized that the alternative addition of organometallic reagents to an α-amino imine derived from a chiral-pool precursor could be more efficient.

Thus, our synthesis began with Garner aldehyde sulfinimine **18** (Scheme 3A), which, to our knowledge, has not been reported previously. To obtain the correct stereochemistry at the α-carbon in the final product, it was necessary to begin with D-serine. *N*-Boc protection, amidation, and *N*,O-acetonide protection were readily accomplished following known procedures to yield the Weinreb amide **16**.[35] This intermediate was then reduced using $LiAlH_4$ to afford D-Garner aldehyde **17**, which was carried forward without further purification. Keeping in mind the observation of Davis and McCoull that sulfinimine derivatives bearing other Lewis basic sites followed an "open" transition state mechanism,[36] we selected (*R*)-*tert*-butylsulfinamide as the appropriate chiral auxiliary to furnish the desired *syn*-product. Condensation of the auxiliary with **17** using $Ti(OEt)_4$, which Ellman had noted is particularly effective for sterically hindered carbonyls, generated the desired sulfinimine **18** in a 74% yield over 2 steps from **16** (Scheme 3A).[37]

To test the diastereoselectivity of the addition reaction, as well as the remainder of the synthetic operations, we elected to first utilize methyl Grignard in a new preparation of (2*S*,3*R*)-methyl-Dap **4** (Scheme 3B). Utilizing Ellman's standard procedure,[38] **18** was reacted with MeMgBr at −78 °C to afford a 7:1 mixture of diastereomers as determined by UPLC−HRMS. The major product was purified and assigned as **19**, although determination of the absolute configuration was not possible at this stage. To verify the assigned stereochemistry, **19** was carried forward to final amino acid **4**, a known compound. Global deprotection of the labile groups was accomplished by acidic methanolysis, and the crude product was reprotected to give the doubly Boc-protected **20**. Oxidation of the primary alcohol to the carboxylic acid was accomplished using Jones' reagent, which was then protected as the *tert*-butyl ester **21** to aid purification. A final, global acid deprotection and anion exchange yielded **4**, whose spectral data were fully consistent with the literature.[39]

https://doi.org/10.1021/jacsau.5c00231
JACS Au 2025, 5, 1992−2003

Scheme 3. Improved Synthesis of (2*S*,3*R*)-MethylDap and (2*S*,3*R*)-VinylDap

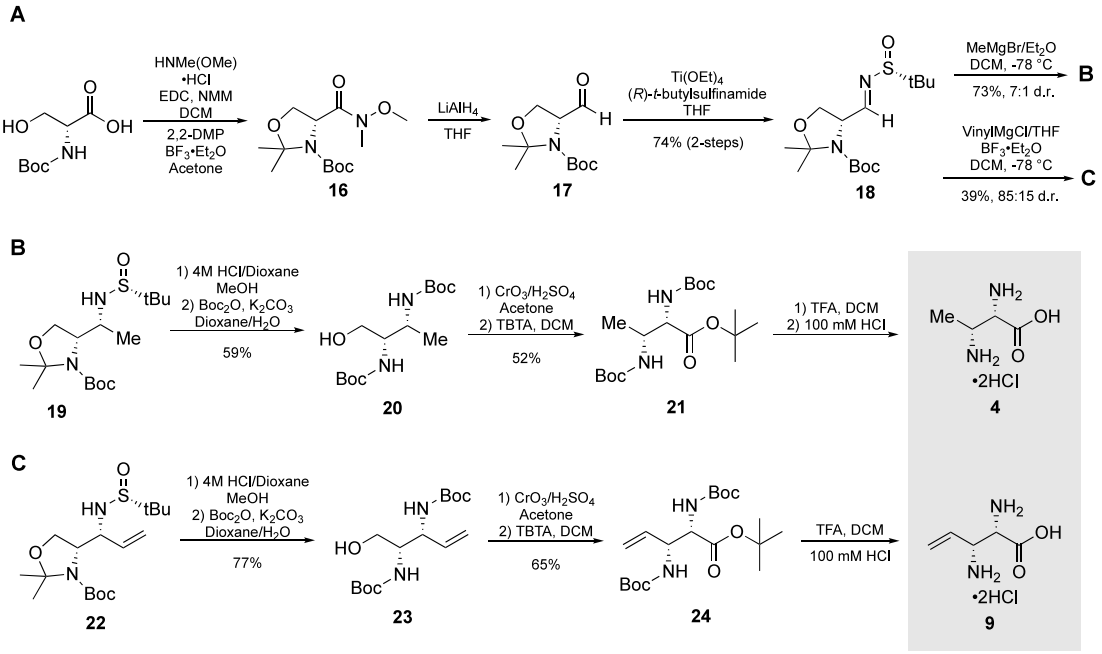

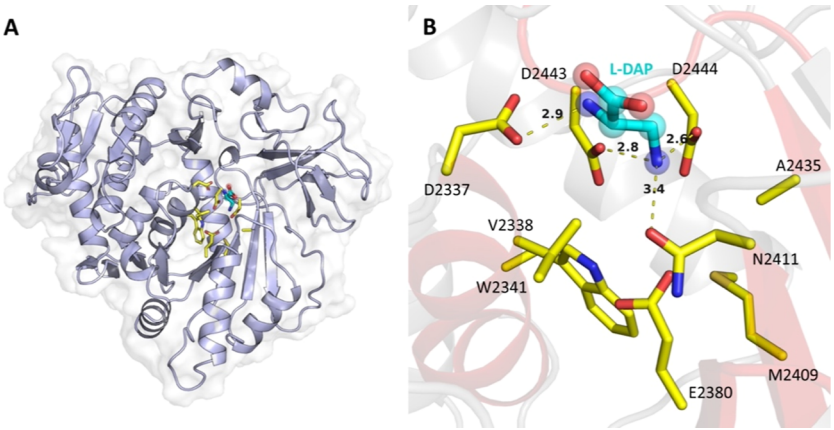

Figure 2. Structures of unliganded and L-DAP-bound SulA3N. (A) Crystal structure of the L-Dap-bound SulA3 N-terminal domain. (C) The L-Dap (cyan carbon) ligand binds to SulA3 and interacts with the specificity code residues (yellow carbon). Substrate binding residues Asp2443 and Asp2444 show an ionic interaction distance of 2.8 and 2.6 Å, respectively, from the side-chain terminal amine of L-Dap, while Asn2411 is within a hydrogen bonding distance of 3.4 Å. The conserved Asp2337 shows interaction with the α-amine of substrate L-Dap, common to all α-amino acid binding adenylation domains.

Having validated this strategy for the diastereoselective construction of L-Dap derivatives, we turned our focus to the synthesis of vinyl-Dap **9**. When we repeated the Grignard addition protocol on **18** with vinylMgCl, however, a ca. 1:1 mixture of diastereomers was obtained. Davis and McCoull had noted that Lewis acid supplementation in the addition reaction is reported to improve diastereoselectivity by precomplexing the sulfinimine.[36] When two equivalents of $BF_3{\cdot}Et_2O$ were added to the reaction prior to addition of the Grignard reagent, a ca. 3:1 d.r. was obtained. This improvement in diastereoselectivity prompted us to carry out a brief optimization study (Table S3). Empirical variation of solvents and concentration led to the 85:15 outcome shown in Scheme 3C. The major diastereomer, which we assigned as **22**, was carried forward using the same conditions as before to afford **24**, which matched the characterization of this compound prepared by our earlier synthetic route.[8] Global deprotection to yield **9** further confirmed the identity of this product. The improved synthetic sequence could be carried out on a multigram scale to generate **24** in only 9 steps from commercially available Boc-D-serine.

Experimental Structures of SulA3 Illustrate a Novel Dap-Binding Pocket

In parallel with these initial engineering experiments and supporting modeling efforts with AlphaFold2 structures of SulA3, we attempted to crystallize full-length SulA3 with and without Dap bound. The full-length adenylation domain, composed of residues Gly2121−Ala2651, was functional[10] but failed to crystallize. Adenylation domains and adenylating enzymes have a long history of biochemical and structural study.[27,40−42] Using established gene cut sites at a conserved hinge region in these proteins, the N-terminal subdomains (also called A_{core}) are known to bind their native substrates and ATP and can be crystallized to give accurate structural

https://doi.org/10.1021/jacsau.5c00231
JACS Au 2025, 5, 1992−2003

Scheme 4. Overview of the Synthesis of AMS Derivatives of (2*S*,3*R*)-MethylDap and (2*S*,3*R*)-VinylDap

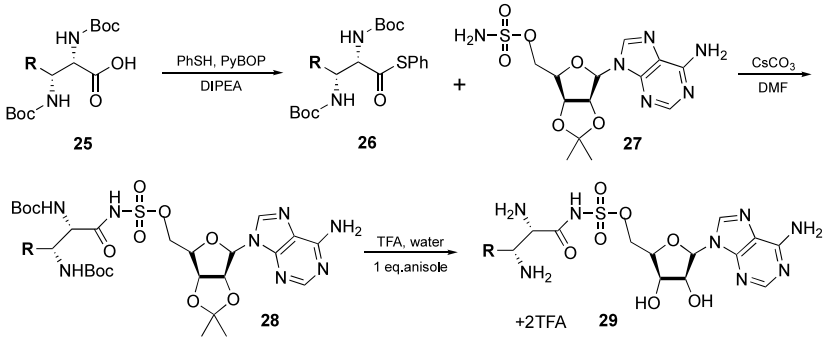

information.[30,40,43,44] Following these precedents, the N-terminal core of SulA3 (denoted SulA3N, composed of residues Pro2124−Lys2545), terminating before the hinge residue at Asp2546 that connects the N-terminal (A_{core}) and C-terminal (A_{sub}) domains, was successfully expressed and cocrystallized with L-Dap.

The structure of the A_{core} domain of SulA3 bound to the native substrate L-Dap was determined at 1.5 Å by using an AlphaFold2 model as the molecular replacement search model. The crystal structure showed one protein chain per asymmetric unit and revealed a typical acyl-CoA synthetase fold (Figure 2). Efforts to solve the structure of SulA3 with alternate diamino acids proved unsuccessful, which we attributed to the lower affinity for these ligands.[11]

Similar to other NRPS adenylation domains, SulA3N showed an important interaction of conserved Asp2337 with the α-amine of the ligand. Among the three anionic amino acids predicted to interact with the C3 amine, only the two aspartic acid residues Asp2443 and Asp2444 formed charged interactions with the L-Dap C3 amine with distances of 2.8 and 2.6 Å, respectively. Asn2411, predicted to form a part of the active site but without precedent from other diamino acid binding homologues, additionally forms a hydrogen bond to the terminal β-amine. The proximity of Asn2411 to the substrate provides a plausible explanation for the impact of the N2411T mutation. Replacement of Asn2411 with threonine likely still enables a hydrogen bonding interaction with the C3 amine, which might reorient slightly to provide extra space that enables the accommodation of the larger (3*R*)-methyl analog. Preliminary experiments with other substitutions to Asn2411 including a serine failed to show any further improvement.

With access to the binding mode for SulA3N to L-Dap, we compared the structure with other NRPS adenylation domains that bind to diamine substrates. We first compared the SulA3 structure to a family of cationic homo polyamino acid (CHPA) synthetases that produce polymers of diamino acids with isopeptide linkages between the side chain amines and the carboxylate.[45−47] Comparison of the L-Dap-bound SulA3 structure to known diamino acid-bound adenylation domain structures of polyornithine synthetase (PosA)[48] and polylysine synthetase (PLs)[49] revealed a striking difference in the binding mode of the substrate side chain. The PosA and PLs adenylation structures with longer diamino acids revealed the interaction of the ligand side chain terminal amine with a conserved glutamate residue and other supporting residues. Prior studies show a loss of activity upon mutation of either the conserved glutamate or the α-amino acid interacting aspartic acid to alanine but not from mutation of other supporting residues,[48] supporting a critical role of the glutamate residue for side chain interaction. In contrast, the L-Dap side-chain amine in SulA3N was too short to form a hydrogen bond with Glu2380 (Figure 2B). The finding suggests that the two Asp residues in SulA3 may function as anchors for the side chain instead of the Glu residue common to longer diamino acid side chains.

Structure of SulA3N and a (2*S*,3*S*)-MethylDap-AMS Mimic of the Bound Substrate Acyladenylate

While the SulA3N protein provided a high-resolution view of the L-Dap ligand, we wished to explore the structure bound to methyl- and vinyl-Dap. As noted above, structures of multiple crystals obtained by cocrystallization or soaking with either larger analogue failed to show active-site density consistent with the ligands. Therefore, to provide the foundation for future directed evolution campaigns to improve methyl- and vinyl-Dap affinity and activation by SulA3N, we sought alternate ligands. It has been observed that acyl adenylates bind 10^2 to 10^3 times more tightly to their adenylating enzymes than their free carboxylic acids.[50] In recognition of this behavior, multiple adenylation domains have been structurally characterized bound to their cognate 5′-*O*-sulfamoyl adenosines (AMS), which represent close bisubstrate analogues and potent, tight-binding inhibitors to give cocrystal structures.[44,51−55]

We used (2*S*,3*R*)-methylDap and (2*S*,3*R*)-vinylDap intermediate carboxylic acids **25** (R = CH_3 or vinyl, Scheme 4) obtained after Jones oxidation of **20** or **23**, respectively (Scheme 3B,C), and activated them as their corresponding thiophenyl esters **26** for direct reaction under mildly alkaline conditions with the protected adenosylsulfamate **27** as reported in the literature.[56−59] The coupled methylDap and vinylDap-protected AMS products **28** (R = CH_3 or vinyl) were obtained as single peaks upon reverse-phase chromatography and treated with aqueous TFA and 1 equiv of anisole. In both cases, NMR analysis of the diamino acid sulfamates revealed a 3:2 mixture of diastereomers. Epimerization at the α-carbon was traced to the $CsCO_3$-mediated coupling reaction to AMS products **29** (R = CH_3 or vinyl). Modification of conditions and acyl leaving group did not improve the overall stereochemical outcome.

Co-crystallization of SulA3N with methylDap-AMS and vinylDap-AMS was performed with the expectation that an intrinsic affinity for the native L-isomer would prevail. This stereochemical preference was indeed observed for methylDap-AMS. On the other hand, no electron density was seen for vinylDap AMS in multiple SulA3N crystals. The structure solution of the methylDap-AMS complex was performed using the unliganded structure as a search model and with one

https://doi.org/10.1021/jacsau.5c00231
JACS Au 2025, 5, 1992−2003

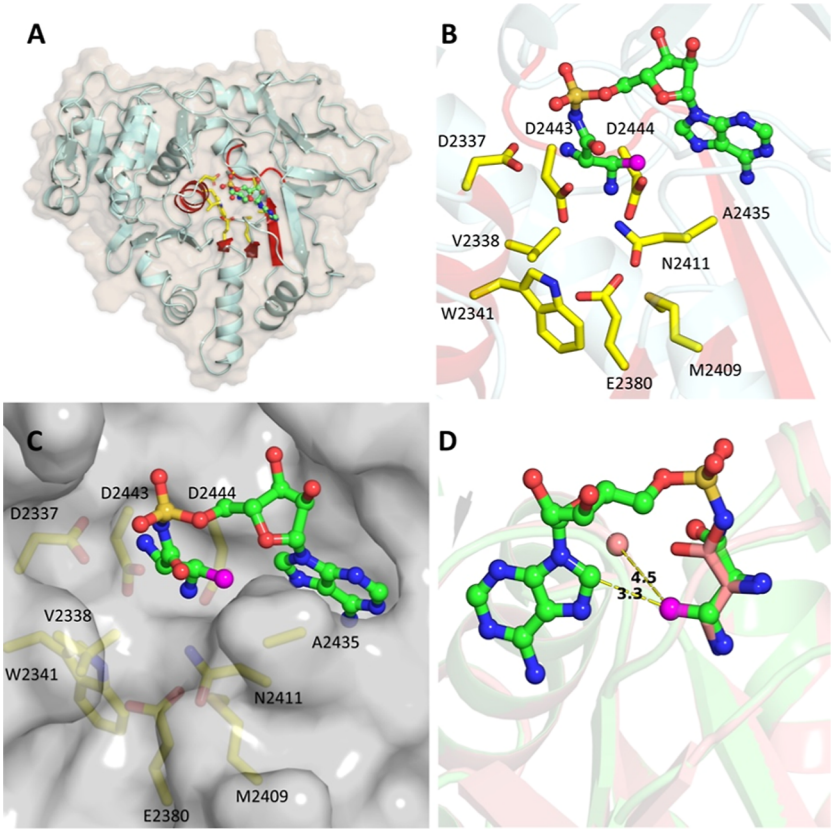

Figure 3. Structure of methyl-DAP-AMS-bound SulA3. (A,B) Crystal structure of the methylDAP-AMS-bound SulA3 N-terminal domain. The ligand methylDAP-AMS (green carbons) interacts with substrate-binding residues of SulA3 (yellow carbon). The methyl carbon of methylDap-AMS is highlighted in purple, projected toward the adenine base. (C) A surface representation of the substrate-binding pocket of SulA3 presents a constrained binding pocket. (D) An overlay of the Dap molecule (salmon) and methylDap-AMS (green) ligands from experimental structures highlights the proximity of the methyl group to the adenine ring and the main chain of Gly2412 (salmon sphere).

	BGC	Specificity residues										Substrate
		1	2	3	4	5	6	7	8	9	10	
Mode 1	*Streptomyces albulus* PD-1 (EXU85975.1)	D	F	**E**	Y	V	G	T	V	T	K	Dap *
	Streptomyces celluloflavus (BCD58482.1)	D	F	**E**	C	L	S	A	V	T	K	Dab *
	Streptoalloteichus hindustanus (WP_083959783.1)	D	F	**E**	C	L	S	C	V	S	K	D-Dab *
	PosA_A, *Acinetobacter baumannii* (ATY43264.1)	D	M	**E**	H	N	G	T	V	S	K	Orn *
	Streptomyces albulus (pls) (BAG68864.1)	D	A	**E**	S	I	G	T	V	V	K	Lys *
	Streptoalloteichus hindustanus (WP_234995776.1)	D	G	**E**	S	V	S	V	V	N	K	β-Lys *
Mode 2	Polymyxin synthetase PmxE_module 1 @	D	V	G	**E**	I	S	S	I	**D**	K	Dab *
	BacB_Module 5 (WP_144531521.1)	D	V	G	**E**	L	M	S	V	**D**	K	Orn
	Paenibacterin_ Module 1 (AGM16412.1)	D	V	G	**E**	I	S	S	V	**D**	K	Orn
	Cupriachelin, Module 3 (CAJ96472.1)	D	I	W	**E**	L	T	A	D	**D**	K	Dab
	Paenibacterin_ Module 7 (AGM16413.1)	D	V	G	**D**	A	V	S	I	**D**	K	Lys
	VioF_A (AAP92496.1)	D	A	Q	**D**	L	A	I	V	**D**	K	Dap
Mode 3	SulM_A3, *Paraburkholderia acidicola* (ASU43976.1)	D	V	W	E	M	N	A	**D**	**D**	K	Dap *
	Flavobacterium sp. Leaf82 (ASF10_RS08290)	D	I	W	E	I	N	T	**D**	**D**	K	Dap #
	Agrobacterium tumefaciens (KY452017.1)	D	I	W	E	I	T	A	**D**	**D**	K	Dap #
	Chryseobacterium sp. G0240 (EGI16_RS09720)	D	I	W	E	V	N	T	**D**	**D**	K	Dap #
	Saccharopolyspora hirsute (WP_150066361.1)	D	I	W	Q	S	T	V	**D**	**D**	K	Dap #
	Tenacibaculum agarivorans (WP_083629583.1)	D	I	W	Q	L	T	A	**D**	**D**	K	Dap #

Figure 4. Sequence comparison of multiple binding modes for diamino acid substrates in NRPS adenylation domains. Numbers 1 to 10 show the positions of residues in the specificity residues for NRPS adenylation domains. The conserved aspartate in position 1 coordinates the α-amine. The glutamate residue experimentally validated to be important for substrate side chain amine binding is highlighted in mode 1. Anionic residues in modes 2 and 3 important for substrate binding are also highlighted, along with characterized substrates (Dap, L-2,3-diaminopropionate; Dab, L-2,4-diaminobutyrate; D-Dab, D-2,4-diaminobutyrate; Orn, L-ornithine; Lys: L-lysine; β-Lys: β-L-lysine; 5hfOrn: 5-hydroxyformyl-L-ornithine). The numbering of SulA3 specificity code residues is as follows: Asp2337, Val2338, Trp2341, Glu2380, Met2409, Asn2411, Ala2435, Asp2443, and Asp2444. Substrates are indicated on the basis of experimentally verified substrates (*), homology to the Dap binding residues of SulA3 (#), or reported literature for the biosynthetic gene cluster. The module definition refers to a full biosynthetic gene cluster. The PmxE sequence (@) was reported recently and biochemically analyzed.[60]

https://doi.org/10.1021/jacsau.5c00231
JACS Au 2025, 5, 1992−2003

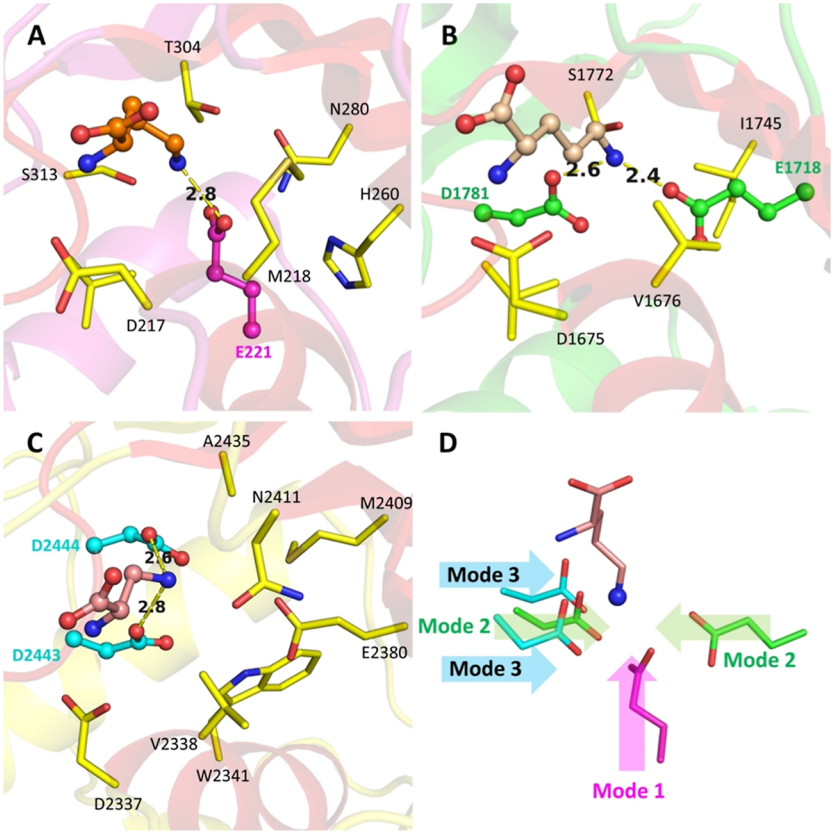

Figure 5. Structural analysis of multiple modes of diamino acid binding in the adenylation domain. (A) The PosA adenylation domain that binds L-ornithine (PDB ID: 8G96) represents mode 1. (B) A model of the gramicidin module 5 adenylation domain bound to L-ornithine as modeled by Chai-1 is used to represent mode 2. (C) SulA3 binding to L-Dap from the present study (PDB 9N1V) is representative of mode 3. (D) Superimposed anionic residues that serve as anchors are highlighted, approaching the side-chain amine (blue) from three orthogonal directions (note: Important residues and substrates are shown as ball and stick models for A, B, and C).

protein chain per asymmetric unit (Figure 3). The methylDap-AMS bound to the SulA3 core domain in a pose that mimicked the position of free L-Dap (Figure 3D). Similar interactions in SulA3N to those observed with L-Dap alone were noted. The adenosine and the ribose moieties were found to be positioned in the canonical pocket as observed for other adenylation domains.[40]

Analysis of the substrate pocket with methylDap-AMS bound revealed a constrained substrate. The ligand-bound structure illustrates that the active-site pocket is tightly positioned with the methyl group directed toward the adenosine moiety. This finding provides a likely explanation for why the vinylDap-AMS could not be captured in the SulA3 pocket and why functional assays, including with active-site mutant enzymes, failed to improve activity. The interactions of the β-amine with the two aspartic acid side chains fix the position of C3, forcing the methyl group in methylDap to orient toward the adenine ring. As the adenine is bordered by the side chain of Tyr2436 on one side and the tripeptide formed by the main chain atoms of Gly2412−Glu2413−Thr2414 on the other, the methyl group is the largest substituent that can be added to the Dap (Figure 3C). This observation implies that additional efforts to expand the binding pocket for vinylDap or larger substrates may require a larger reorganization of the pocket such that the aspartic acid residues are repositioned to direct the C3 group away from the nucleotide ring.

Sequence Analysis of the Diamino Acid-Activating NRPS Adenylation Domain

The experimental structures of Dap and methylDap-AMS bound to SulA3 illustrate that the binding pose projects the C3 carbon toward the adenine ring, limiting the size of groups that can be appended onto the natural Dap substrate. To explore the potential to incorporate larger substrates into SulA3, we examined other NRPS adenylation domains that exhibit alternate modes of binding to diamino acid substrates. This approach could allow us to identify alternate binding modes for L-Dap that orient the substrate into available space to lengthen the group to larger analogues. A detailed sequence analysis of adenylation domains was performed to better understand the orientation of the negatively charged residue anchoring the side chain terminal amine of the diamino acid substrates. Structure-based sequence alignment of adenylation domains that activate multiple diamino acids was performed. The substrate binding residues[25,26] were extracted and further aligned to determine the positions of the negatively charged residues (Figure 4).

On the basis of the position of negatively charged residues, we identified three distinct modes for diamino acid substrate binding (Figure 5). In the first mode, represented by the NRPS-like cationic homopolymeric amino acid (CHPA) synthetases like PosA or Pls,[45−47] a critical glutamate residue at position 3 of the specificity code forms part of the adenylation domain. Structural and biochemical characterization of PosA, a δ-polyornithine synthesizing enzyme, has

https://doi.org/10.1021/jacsau.5c00231
JACS Au 2025, 5, 1992−2003

confirmed the role of Glu in anchoring the side chain amine.[48] We consider this glutamate position to be a hallmark of binding mode 1, which requires only one Glu residue for binding various diamino acids from three-carbon L-Dap to six-carbon L-lysine. Detailed sequence analysis of adenylation domains from this family of NRPS-like proteins revealed the roles of other residues in determining the chain length of the recognized substrates. Adenylation domains from proteins other than the CHPA synthetase family also showed binding mode 1, including the adenylation domains from BGCs of pyoverdine, sessilin A, jessenipeptin, and syringomycin, which all show a Glu residue at position 3.

Mode 2 is defined by the presence of two negatively charged residues, either glutamate or aspartate at positions 4 and 9, respectively, or aspartate residues at both positions. Since no structures of adenylation domains from this group are available, AlphaFold3 models were used for analysis. Structural analysis demonstrated that both residues could play important roles in binding diamino acids. Binding mode 2 can also accommodate diamino acids of various chain lengths such as mode 1. The adenylation domains from various BGCs like gramicidin, bacitracin, polymyxin, and paenibacterin showed binding mode 2. A recent report examined the adenylation domain specificity in the polymyxin NRPS from *Paenibacillus polymyxa* NBRC2030.[60] Here, six of ten NRPS modules incorporate a molecule of 2,4-diaminobutyrate in the formation of cationic antibiotic polymyxin. Four adenylation domains that present the specificity code of DVGEISSIDK were examined, highlighting the conserved glutamate at position 4 and the aspartic acid at position 9. Mutation of either of these residues to alanine resulted in background activity with a variety of diamino acids ranging from Dab to lysine.[60]

A third binding architecture is seen in mode 3, represented by SulA3, which has two Asp residues at positions 8 and 9, while another Glu residue at position 4 that may be redundant appears farther from the pocket. In preliminary mutagenesis experiments, mutation of the two aspartic acid residues had a more dramatic impact than mutation of glutamate on adenylation activity with L-Dap (data not shown). All three mutants showed modest activity with serine and threonine. Interestingly, we could not find mode 3 in any known BGCs other than the sulfazecin BGC analyzed in the present study. Since no other BGC has shown mode 3, a BLAST search was performed to find more adenylation domains exhibiting the mode 3 motif. Several sequences with similarities greater than 70% showed the mode 3 signature, but with more variability at positions 5, 6, and 7, which may not be playing important roles in substrate binding (Figure 4). The identified homologues all contain a substitution of isoleucine for valine at position 2. Several homologues replace the glutamate with a glutamine, also speaking of its limited role in the activation of Dap.

While mode 3 of SulA3 that directs the methyl group toward the nucleotide moiety prevents the extension of the substrate, mode 1 adopted by PosA may alter the binding pose of the alkyl chain, enabling the use of analogues of L-Dap, with ethyl, vinyl, or longer groups adopting space in the pocket. In the PosA structure bound to the canonical substrate L-ornithine as well as D-ornithine,[48] the configuration of the carbon atoms equivalent to C2 and C3 of L-Dap rotates to adopt a new orientation, directing them toward a solvent-filled cavity bound by Met218 and Gly283. The identification of these alternate modes in which adenylation domains bind to diamino acid substrates offers a potential route to the further engineering of SulA3. Reorienting an alkyl chain in a binding pocket, particularly where the α-amine and carboxylate of the substrate are in the fixed position required by the chemistry, likely would not be easy and would require further evolutionary screening and selection in place of a rational point mutation approach. Nonetheless, adoption of features from PosA into a SulM mutant may be a first step toward engineering SulA3 to allow activity with larger L-Dap analogues that could form sulfazecin variants.

CONCLUSIONS

Diamino acids appear prominently in NRPS products, notably in antibiotics and siderophores. Apart from the occurrence of lysine and ornithine, 2,3-diaminobutyrate (Dap) is the simplest and is derived in two metabolic steps biosynthetically from 3-phosphoserine, a universal component of central metabolism.[11] It plays an essential role in the formation of the monobactam family of β-lactam antibiotics, which have an increasingly important clinical function for their intrinsic resistance to metallo-β-lactamases (MBLs). Our initial focus was to engineer the SulM A3 adenylation domain that activates Dap for sulfazecin biosynthesis employing AlphaFold models of the active site and structure-based decisions about rational mutagenesis with the goal in mind to improve binding and selectivity for L-Dap derivatives bearing functionalizable sites at the (3*R*)-position, for example, a vinyl group. It was previously known that monobactams elaborated by even small substituents at the corresponding (4*R*)-position on the β-lactam ring have enhanced antibiotic properties.[18,19] We soon realized that the precise bond angle and the distance between envisioned substituents and active-site residues would be critical to success. We employed high-resolution X-ray structures of SulA3N with L-Dap and (2*S*,3*R*)-methylDap-AMS bound to clearly define the binding pose. Critically, the orientation of the (3*R*)-substituent was unambiguously mapped and identified limitations in the SulA3 binding strategy that prevented the incorporation of larger Dap analogues.

Despite over two decades of determined effort, including efforts by us and others that have shown improvements in activity,[43,61−65] reprograming NRPS A domains remains a nontrivial but worthy goal. The use of biocatalytic approaches to make novel NRPS products with important bioactivities remains a challenging but exciting approach to access analogues of these molecules that are often synthetically challenging due to their large size and the presence of multiple stereocenters. The importance of diamino acids to NRPS-derived peptides and natural products, especially monobactam antibiotics, underscores the value of high-quality X-ray structures, particularly with substrate(s) bound to further advance these studies.

ASSOCIATED CONTENT

Data Availability Statement

The structures of SulA3N have been deposited with the worldwide Protein Data Bank (SulA3N bound to L-DAP, 9N1U; SulA3N bound to methyl-L-DAP-AMS, 9N1V).

Supporting Information

The Supporting Information is available free of charge at https://pubs.acs.org/doi/10.1021/jacsau.5c00231.

https://doi.org/10.1021/jacsau.5c00231
JACS Au 2025, 5, 1992−2003

General synthetic methods, materials, details of synthetic steps, and NMR and mass spectrometric characterizations of new compounds; general microbiological methods and primers used in mutagenesis experiments; and protein crystallization and crystallographic data (PDF)

AUTHOR INFORMATION

Corresponding Authors

Andrew M. Gulick − *Department of Structural Biology, Jacobs School of Medicine and Biomedical Sciences, University at Buffalo, Buffalo, New York 14203, United States;* orcid.org/0000-0003-4238-7453; Email: amgulick@buffalo.edu

Craig A. Townsend − *Department of Chemistry, Johns Hopkins University, Baltimore, Maryland 21218, United States;* orcid.org/0000-0003-2795-7585; Email: ctownsend@jhu.edu

Authors

Lukas Kahlert − *Department of Chemistry, Johns Hopkins University, Baltimore, Maryland 21218, United States*

Ketan D. Patel − *Department of Structural Biology, Jacobs School of Medicine and Biomedical Sciences, University at Buffalo, Buffalo, New York 14203, United States*

Michael S. Lichstrahl − *Department of Chemistry, Johns Hopkins University, Baltimore, Maryland 21218, United States*

Rongfeng Li − *Department of Chemistry, Johns Hopkins University, Baltimore, Maryland 21218, United States;* orcid.org/0000-0001-8879-3241

Chengkun He − *Department of Chemistry, Johns Hopkins University, Baltimore, Maryland 21218, United States;* orcid.org/0000-0002-7127-0097

Complete contact information is available at: https://pubs.acs.org/10.1021/jacsau.5c00231

Author Contributions

[§]L.K. and K.D.P. contributed equally to the project. M.S.L. designed the improved synthesis of (2*S*,3*R*)-vinylDap and implemented it with L.K., and C.H. L.K. generated the initial AlphaFold model of SulA3 and carried out the rational mutagenesis experiments. C.H. and L.K. carried out the synthesis of the AMS derivatives of (2*S*,3*R*)-methylDap and (2*S*,3*R*)-vinylDap. R.L. designed and carried out the expression and purification of SulA3, SulA3N, and all truncated constructs. K.D.P. crystallized and determined the experimental structure of SulA3N in the presence of all ligands. C.A.T. and A.M.G. conceived the study and provided financial support and guidance throughout. C.A.T. and A.M.G. initiated writing of the paper with contributions and analysis from all authors to achieve the completed version.

Notes

The authors declare no competing financial interest.

ACKNOWLEDGMENTS

The investigation was supported by NIH grants GM136235 (to A.M.G.) and AI121072 (to C.A.T.). Diffraction data were collected at the SSRL. Use of the Stanford Synchrotron Radiation Lightsource, SLAC National Accelerator Laboratory, is supported by the U.S. Department of Energy, Office of Science, Office of Basic Energy Sciences under Contract No. DE-AC02-76SF00515. The SSRL Structural Molecular Biology Program is supported by the DOE Office of Biological and Environmental Research, and by the National Institutes of Health, National Institute of General Medical Sciences (including P41GM103393). The contents of this publication are solely the responsibility of the authors and do not necessarily represent the official views of the NIGMS or NIH. Diffraction data were also collected at APS (Advanced Photon Source, Lemont, IL 60439, USA). GM/CA@APS has been funded by the National Cancer Institute (ACB-12002) and the National Institute of General Medical Sciences (AGM-12006, P30GM138396). This research used resources from the Advanced Photon Source, a U.S. Department of Energy (DOE) Office of Science User Facility operated for the DOE Office of Science by the Argonne National Laboratory under Contract No. DE-AC02-06CH11357. L.K. acknowledges financial support from the Deutsche Forschungsgemeinschaft (DFG, German Research Foundation)—492438365.

REFERENCES

(1) Rinehart, K. L. Mutasynthesis of New Antibiotics. *Pure Appl. Chem.* **1977**, *49* (9), 1361−1384.

(2) Shier, W. T.; Rinehart, K. L.; Gottlieb, D. Preparation of four new antibiotics from a mutant of Streptomyces fradiae. *Proc. Natl. Acad. Sci. U.S.A.* **1969**, *63* (1), 198−204.

(3) Kennedy, J. Mutasynthesis, chemobiosynthesis, and back to semi-synthesis: combining synthetic chemistry and biosynthetic engineering for diversifying natural products. *Nat. Prod. Rep.* **2008**, *25* (1), 25−34.

(4) Weissman, K. J. Mutasynthesis - uniting chemistry and genetics for drug discovery. *Trends Biotechnol.* **2007**, *25* (4), 139−142.

(5) Gregory, M. A.; Petkovic, H.; Lill, R. E.; Moss, S. J.; Wilkinson, B.; Gaisser, S.; Leadlay, P. F.; Sheridan, R. M. Mutasynthesis of rapamycin analogues through the manipulation of a gene governing starter unit biosynthesis. *Angew. Chem., Int. Ed. Engl.* **2005**, *44* (30), 4757−4760.

(6) Denoya, C. D.; Fedechko, R. W.; Hafner, E. W.; McArthur, H. A.; Morgenstern, M. R.; Skinner, D. D.; Stutzman-Engwall, K.; Wax, R. G.; Wernau, W. C. A second branched-chain alpha-keto acid dehydrogenase gene cluster (bkdFGH) from Streptomyces avermitilis: its relationship to avermectin biosynthesis and the construction of a bkdF mutant suitable for the production of novel antiparasitic avermectins. *J. Bacteriol.* **1995**, *177* (12), 3504−3511.

(7) Bozhuyuk, K. A.; Micklefield, J.; Wilkinson, B. Engineering enzymatic assembly lines to produce new antibiotics. *Curr. Opin. Microbiol.* **2019**, *51*, 88−96.

(8) Lichstrahl, M. S.; Kahlert, L.; Li, R.; Zandi, T. A.; Yang, J.; Townsend, C. A. Synthesis of functionalized 2,3-diaminopropionates and their potential for directed monobactam biosynthesis. *Chem. Sci.* **2023**, *14* (14), 3923−3931.

(9) Li, R.; Oliver, R. A.; Townsend, C. A. Identification and Characterization of the Sulfazecin Monobactam Biosynthetic Gene Cluster. *Cell Chem. Biol.* **2017**, *24* (1), 24−34.

(10) Oliver, R. A.; Li, R.; Townsend, C. A. Monobactam formation in sulfazecin by a nonribosomal peptide synthetase thioesterase. *Nat. Chem. Biol.* **2018**, *14* (1), 5−7.

(11) Li, R.; Lichstrahl, M. S.; Zandi, T. A.; Kahlert, L.; Townsend, C. A. The dabABC operon is a marker of C4-alkylated monobactam biosynthesis and is responsible for (2S,3R)-diaminobutyrate production. *iScience* **2024**, *27* (3), 109202.

(12) Süssmuth, R. D.; Mainz, A. Nonribosomal Peptide Synthesis-Principles and Prospects. *Angew. Chem., Int. Ed. Engl.* **2017**, *56* (14), 3770−3821.

(13) Patel, K. D.; MacDonald, M. R.; Ahmed, S. F.; Singh, J.; Gulick, A. M. Structural advances toward understanding the catalytic activity

and conformational dynamics of modular nonribosomal peptide synthetases. *Nat. Prod. Rep.* **2023**, *40* (9), 1550−1582.
(14) Walsh, C. T. Insights into the chemical logic and enzymatic machinery of NRPS assembly lines. *Nat. Prod. Rep.* **2016**, *33* (2), 127−135.
(15) Patel, K. D.; Oliver, R. A.; Lichstrahl, M. S.; Li, R.; Townsend, C. A.; Gulick, A. M. The structure of the monobactam-producing thioesterase domain of SulM forms a unique complex with the upstream carrier protein domain. *J. Biol. Chem.* **2024**, *300* (8), 107489.
(16) Kreitler, D. F.; Gemmell, E. M.; Schaffer, J. E.; Wencewicz, T. A.; Gulick, A. M. The structural basis of N-acyl-alpha-amino-beta-lactone formation catalyzed by a nonribosomal peptide synthetase. *Nat. Commun.* **2019**, *10* (1), 3432.
(17) Schaffer, J. E.; Reck, M. R.; Prasad, N. K.; Wencewicz, T. A. β-Lactone formation during product release from a nonribosomal peptide synthetase. *Nat. Chem. Biol.* **2017**, *13* (7), 737−744.
(18) Imada, A.; Kondo, M.; Okonogi, K.; Yukishige, K.; Kuno, M. In vitro and in vivo antibacterial activities of carumonam (AMA-1080), a new N-sulfonated monocyclic beta-lactam antibiotic. *Antimicrob. Agents Chemother.* **1985**, *27* (5), 821−827.
(19) Reck, F.; Bermingham, A.; Blais, J.; Capka, V.; Cariaga, T.; Casarez, A.; Colvin, R.; Dean, C. R.; Fekete, A.; Gong, W.; Growcott, E.; Guo, H.; Jones, A. K.; Li, C.; Li, F.; Lin, X.; Lindvall, M.; Lopez, S.; McKenney, D.; Metzger, L.; Moser, H. E.; Prathapam, R.; Rasper, D.; Rudewicz, P.; Sethuraman, V.; Shen, X.; Shaul, J.; Simmons, R. L.; Tashiro, K.; Tang, D.; Tjandra, M.; Turner, N.; Uehara, T.; Vitt, C.; Whitebread, S.; Yifru, A.; Zang, X.; Zhu, Q. Optimization of novel monobactams with activity against carbapenem-resistant Enterobacteriaceae - Identification of LYS228. *Bioorg. Med. Chem. Lett.* **2018**, *28* (4), 748−755.
(20) Kahlert, L.; Lichstrahl, M. S.; Townsend, C. A. Colorimetric Determination of Adenylation Domain Activity in Nonribosomal Peptide Synthetases by Using Chrome Azurol S. *Chembiochem* **2023**, *24* (5), No. e202200668.
(21) Adams, P. D.; Afonine, P. V.; Bunkoczi, G.; Chen, V. B.; Davis, I. W.; Echols, N.; Headd, J. J.; Hung, L. W.; Kapral, G. J.; Grosse-Kunstleve, R. W.; McCoy, A. J.; Moriarty, N. W.; Oeffner, R.; Read, R. J.; Richardson, D. C.; Richardson, J. S.; Terwilliger, T. C.; Zwart, P. H. PHENIX: a comprehensive Python-based system for macromolecular structure solution. *Acta Crystallogr., Sect. D: Biol. Crystallogr.* **2010**, *66* (2), 213−221.
(22) McCoy, A. J.; Grosse-Kunstleve, R. W.; Adams, P. D.; Winn, M. D.; Storoni, L. C.; Read, R. J. Phaser crystallographic software. *J. Appl. Crystallogr.* **2007**, *40*, 658−674.
(23) Emsley, P.; Cowtan, K. Coot: model-building tools for molecular graphics. *Acta Crystallogr., Sect. D: Biol. Crystallogr.* **2004**, *60* (12), 2126−2132.
(24) Jumper, J.; Evans, R.; Pritzel, A.; Green, T.; Figurnov, M.; Ronneberger, O.; Tunyasuvunakool, K.; Bates, R.; Zidek, A.; Potapenko, A.; Bridgland, A.; Meyer, C.; Kohl, S. A. A.; Ballard, A. J.; Cowie, A.; Romera-Paredes, B.; Nikolov, S.; Jain, R.; Adler, J.; Back, T.; Petersen, S.; Reiman, D.; Clancy, E.; Zielinski, M.; Steinegger, M.; Pacholska, M.; Berghammer, T.; Bodenstein, S.; Silver, D.; Vinyals, O.; Senior, A. W.; Kavukcuoglu, K.; Kohli, P.; Hassabis, D. Highly accurate protein structure prediction with AlphaFold. *Nature* **2021**, *596* (7873), 583−589.
(25) Stachelhaus, T.; Mootz, H. D.; Marahiel, M. A. The specificity-conferring code of adenylation domains in nonribosomal peptide synthetases. *Chem. Biol.* **1999**, *6* (8), 493−505.
(26) Challis, G. L.; Ravel, J.; Townsend, C. A. Predictive, structure-based model of amino acid recognition by nonribosomal peptide synthetase adenylation domains. *Chem. Biol.* **2000**, *7* (3), 211−224.
(27) Heard, S. C.; Winter, J. M. Structural, biochemical and bioinformatic analyses of nonribosomal peptide synthetase adenylation domains. *Nat. Prod. Rep.* **2024**, *41* (7), 1180−1205.
(28) Ishikawa, F.; Nakamura, S.; Nakanishi, I.; Tanabe, G. Recent progress in the reprogramming of nonribosomal peptide synthetases. *J. Pept. Sci.* **2024**, *30* (3), No. e3545.
(29) Eppelmann, K.; Stachelhaus, T.; Marahiel, M. A. Exploitation of the selectivity-conferring code of nonribosomal peptide synthetases for the rational design of novel peptide antibiotics. *Biochemistry* **2002**, *41* (30), 9718−9726.
(30) Niquille, D. L.; Hansen, D. A.; Mori, T.; Fercher, D.; Kries, H.; Hilvert, D. Nonribosomal biosynthesis of backbone-modified peptides. *Nat. Chem.* **2018**, *10* (3), 282−287.
(31) Zhang, K.; Kries, H. Biomimetic engineering of nonribosomal peptide synthesis. *Biochem. Soc. Trans.* **2023**, *51* (4), 1521−1532.
(32) Brown, A. S.; Calcott, M. J.; Owen, J. G.; Ackerley, D. F. Structural, functional and evolutionary perspectives on effective re-engineering of non-ribosomal peptide synthetase assembly lines. *Nat. Prod. Rep.* **2018**, *35* (11), 1210−1228.
(33) Bozhuyuk, K. A. J.; Prave, L.; Kegler, C.; Schenk, L.; Kaiser, S.; Schelhas, C.; Shi, Y. N.; Kuttenlochner, W.; Schreiber, M.; Kandler, J.; Alanjary, M.; Mohiuddin, T. M.; Groll, M.; Hochberg, G. K. A.; Bode, H. B. Evolution-inspired engineering of nonribosomal peptide synthetases. *Science* **2024**, *383* (6689), No. eadg4320.
(34) Viso, A.; Fernandez de la Pradilla, R.; Tortosa, M.; Garcia, A.; Flores, A. Update 1 of: alpha,beta-Diamino acids: biological significance and synthetic approaches. *Chem. Rev.* **2011**, *111* (2), PR1−42.
(35) Smith, M. W.; Snyder, S. A. A concise total synthesis of (+)-scholarisine A empowered by a unique C-H arylation. *J. Am. Chem. Soc.* **2013**, *135* (35), 12964−12967.
(36) Davis, F. A.; McCoull, W. Concise Asymmetric Synthesis of alpha-Amino Acid Derivatives from N-Sulfinylimino Esters. *J. Org. Chem.* **1999**, *64* (10), 3396−3397.
(37) Liu, G.; Cogan, D. A.; Owens, T. D.; Tang, T. P.; Ellman, J. A. Synthesis of enantiomerically pure N-tert-butanesulfinyl Imines (tert-butanesulfinimines) by the direct condensation of tert-butanesulfinamide with aldehydes and ketones. *J. Org. Chem.* **1999**, *64*, 1278−1284.
(38) Cogan, D. A.; Liu, G.; Ellman, J. Asymmetric synthesis of chiral amines by highly diastereoselective 1,2-additions of organometallic reagents to N-tert-butanesulfinyl imines. *Tetrahedron* **1999**, *55*, 8883−8904.
(39) Han, H.; Yoon, J.; Janda, K. D. An efficient asymmetric route to 2,3-diaminobutanoic acids. *J. Org. Chem.* **1998**, *63*, 2045−2048.
(40) Gulick, A. M. Conformational dynamics in the acyl-CoA synthetases, adenylation domains of non-ribosomal peptide synthetases, and firefly luciferase. *ACS Chem. Biol.* **2009**, *4*, 811−827.
(41) Kudo, F.; Miyanaga, A.; Eguchi, T. Structural basis of the nonribosomal codes for nonproteinogenic amino acid selective adenylation enzymes in the biosynthesis of natural products. *J. Ind. Microbiol. Biotechnol.* **2019**, *46* (3−4), 515−536.
(42) Zhang, M.; Peng, Z.; Huang, Z.; Fang, J.; Li, X.; Qiu, X. Functional Diversity and Engineering of the Adenylation Domains in Nonribosomal Peptide Synthetases. *Mar. Drugs* **2024**, *22* (8), 349.
(43) Miyanaga, A.; Cieslak, J.; Shinohara, Y.; Kudo, F.; Eguchi, T. The crystal structure of the adenylation enzyme VinN reveals a unique beta-amino acid recognition mechanism. *J. Biol. Chem.* **2014**, *289* (45), 31448−31457.
(44) Alexander, E. M.; Kreitler, D. F.; Guidolin, V.; Hurben, A. K.; Drake, E.; Villalta, P. W.; Balbo, S.; Gulick, A. M.; Aldrich, C. C. Biosynthesis, Mechanism of Action, and Inhibition of the Enterotoxin Tilimycin Produced by the Opportunistic Pathogen Klebsiella oxytoca. *ACS Infect. Dis.* **2020**, *6* (7), 1976−1997.
(45) Hamano, Y.; Arai, T.; Ashiuchi, M.; Kino, K. NRPSs and amide ligases producing homopoly(amino acid)s and homooligo(amino acid)s. *Nat. Prod. Rep.* **2013**, *30* (8), 1087−1097.
(46) Yamanaka, K.; Maruyama, C.; Takagi, H.; Hamano, Y. Epsilon-poly-L-lysine dispersity is controlled by a highly unusual non-ribosomal peptide synthetase. *Nat. Chem. Biol.* **2008**, *4* (12), 766−772.
(47) Xu, Z.; Sun, Z.; Li, S.; Xu, Z.; Cao, C.; Xu, Z.; Feng, X.; Xu, H. Systematic unravelling of the biosynthesis of poly (L-diaminopropionic acid) in Streptomyces albulus PD-1. *Sci. Rep.* **2015**, *5*, 17400.

https://doi.org/10.1021/jacsau.5c00231
JACS Au 2025, 5, 1992−2003

(48) Patel, K. D.; Gulick, A. M. Structural and functional insights into delta-poly-L-ornithine polymer biosynthesis from Acinetobacter baumannii. *Commun. Biol.* **2023**, *6* (1), 982.
(49) Okamoto, T.; Yamanaka, K.; Hamano, Y.; Nagano, S.; Hino, T. Crystal structure of the adenylation domain from an epsilon-poly-l-lysine synthetase provides molecular mechanism for substrate specificity. *Biochem. Biophys. Res. Commun.* **2022**, *596*, 43−48.
(50) Kim, S.; Lee, S. W.; Choi, E. C.; Choi, S. Y. Aminoacyl-tRNA synthetases and their inhibitors as a novel family of antibiotics. *Appl. Microbiol. Biotechnol.* **2003**, *61* (4), 278−288.
(51) Drake, E. J.; Duckworth, B. P.; Neres, J.; Aldrich, C. C.; Gulick, A. M. Biochemical and structural characterization of bisubstrate inhibitors of BasE, the self-standing nonribosomal peptide synthetase adenylate-forming enzyme of acinetobactin synthesis. *Biochemistry* **2010**, *49* (43), 9292−9305.
(52) Shelton, C. L.; Meneely, K. M.; Ronnebaum, T. A.; Chilton, A. S.; Riley, A. P.; Prisinzano, T. E.; Lamb, A. L. Rational inhibitor design for Pseudomonas aeruginosa salicylate adenylation enzyme PchD. *J. Biol. Inorg. Chem.* **2022**, *27* (6), 541−551.
(53) Reimer, J. M.; Eivaskhani, M.; Harb, I.; Guarne, A.; Weigt, M.; Schmeing, T. M. Structures of a dimodular nonribosomal peptide synthetase reveal conformational flexibility. *Science* **2019**, *366* (6466), No. eaaw4388.
(54) Corpuz, J. C.; Podust, L. M.; Davis, T. D.; Jaremko, M. J.; Burkart, M. D. Dynamic visualization of type II peptidyl carrier protein recognition in pyoluteorin biosynthesis. *RSC Chem. Biol.* **2020**, *1* (1), 8−12.
(55) Corpuz, J. C.; Patel, A.; Davis, T. D.; Podust, L. M.; McCammon, J. A.; Burkart, M. D. Essential Role of Loop Dynamics in Type II NRPS Biomolecular Recognition. *ACS Chem. Biol.* **2022**, *17* (10), 2890−2898.
(56) Finking, R.; Neumuller, A.; Solsbacher, J.; Konz, D.; Kretzschmar, G.; Schweitzer, M.; Krumm, T.; Marahiel, M. A. Aminoacyl adenylate substrate analogues for the inhibition of adenylation domains of nonribosomal peptide synthetases. *Chembiochem* **2003**, *4* (9), 903−906.
(57) Ferreras, J. A.; Ryu, J. S.; Di Lello, F.; Tan, D. S.; Quadri, L. E. Small-molecule inhibition of siderophore biosynthesis in Mycobacterium tuberculosis and Yersinia pestis. *Nat. Chem. Biol.* **2005**, *1* (1), 29−32.
(58) Qiao, C.; Gupte, A.; Boshoff, H. I.; Wilson, D. J.; Bennett, E. M.; Somu, R. V.; Barry, C. E.; Aldrich, C. C. 5′-O-[(N-Acyl)-sulfamoyl]adenosines as Antitubercular Agents that Inhibit MbtA: An Adenylation Enzyme Required for Siderophore Biosynthesis of the Mycobactins. *J. Med. Chem.* **2007**, *50* (24), 6080−6094.
(59) Ishikawa, F.; Kakeya, H. Specific enrichment of nonribosomal peptide synthetase module by an affinity probe for adenylation domains. *Bioorg. Med. Chem. Lett.* **2014**, *24* (3), 865−869.
(60) Nemoto, M.; Ando, W.; Mano, T.; Lee, M.; Yuzawa, S.; Mizuno, T. Identification of Key Amino Acids in the A Domains of Polymyxin Synthetase Responsible for 2,4-Diaminobutyric Acid Adenylation in Paenibacillus polymyxa NBRC3020 Strain. *ACS Chem. Biol.* **2025**, *20* (2), 321−331.
(61) Ishikawa, F.; Miyanaga, A.; Kitayama, H.; Nakamura, S.; Nakanishi, I.; Kudo, F.; Eguchi, T.; Tanabe, G. An Engineered Aryl Acid Adenylation Domain with an Enlarged Substrate Binding Pocket. *Angew. Chem., Int. Ed. Engl.* **2019**, *58* (21), 6906−6910.
(62) Conley, E.; Wadler, C. S.; Bell, B. A.; Lucier, I.; Haynie, C.; Eldred, S.; Nguyen, V.; Bugni, T. S.; Thomas, M. G. Directed Evolution of an Adenylation Domain Alters Substrate Specificity and Generates a New Catechol Siderophore in Escherichia coli. *Biochemistry* **2024**, *63* (23), 3126−3135.
(63) Ishikawa, F.; Nohara, M.; Miyanaga, A.; Kuramoto, S.; Miyano, N.; Asamizu, S.; Kudo, F.; Onaka, H.; Eguchi, T.; Tanabe, G. Biosynthetic Incorporation of Non-native Aryl Acid Building Blocks into Peptide Products Using Engineered Adenylation Domains. *ACS Chem. Biol.* **2024**, *19* (12), 2569−2579.
(64) Ahmed, S. F.; Balutowski, A.; Yang, J.; Wencewicz, T. A.; Gulick, A. M. Expanding the Substrate Selectivity of the Fimsbactin Biosynthetic Adenylation Domain, FbsH. *ACS Chem. Biol.* **2024**, *19* (12), 2451−2461.
(65) Ahmed, S. F.; Gulick, A. M. The Structural Basis of Substrate Selectivity of the Acinetobactin Biosynthetic Adenylation Domain, BasE. *J. Biol. Chem.* **2025**, *301*, 108413.

https://doi.org/10.1021/jacsau.5c00231
JACS Au 2025, 5, 1992−2003